Heliyon 6 (2020) e05294

Contents lists available at ScienceDirect

Heliyon

journal homepage: www.cell.com/heliyon

Research article

Characterizing internal cavity modulation of corn starch microcapsules

David Wulff [a,b], Ariel Chan [c], Qiang Liu [d], Frank X. Gu [c], Marc G. Aucoin [a,b,*]

[a] Department of Chemical Engineering, University of Waterloo, Waterloo, Ontario, N2L 3G1, Canada
[b] Waterloo Institute for Nanotechnology, Waterloo, Ontario, N2L 3G1, Canada
[c] Department of Chemical Engineering & Applied Chemistry, University of Toronto, Toronto, M5S 3E5, Canada
[d] Guelph Research and Development Center, Agriculture and Agri-Food Canada, Guelph, Ontario N1G 5C9, Canada

ARTICLE INFO

Keywords:
Food science
Nanotechnology
Pharmaceutical science
Materials science
Corn starch
Morphology
Partial gelatinization
Structure
Swelling
Tunable microcapsule

ABSTRACT

Swelling of normal corn starch granules through heating in water leads to enlargement of the starch particles and a corresponding increase in internal cavity size. Through control of the swelling extent, it is possible to tune the size of the internal cavity for the starch microcapsules (SMCs). The swelling extent can be controlled through regulation of the swelling time and the swelling temperature. Since the swelling extent is correlated with particle size and solubility, these aspects may also be controlled. Imaging the SMCs at increasing levels of swelling extent using scanning electron microscopy (SEM) allowed for the internal cavity swelling process to be clearly observed. Brightfield and polarizing light microscopy validated the SEM observations. Confocal laser scanning microscopy provided further validation and indicated that it is possible to load the SMCs with large molecules through diffusion. The highly tunable SMCs are novel microparticles which could have applications in various industries.

1. Introduction

Starch is one of the most widely used biopolymers. In addition to its primary use as an energy source in food, starch has been used, typically with modifications, in the pharmaceutical, packaging, paper, plastic, cosmetic, and medical industries (Liu, 2005). Despite extensive research over the past many decades, starch structure is still not fully understood (Bertoft, 2017; Zhu, 2018). Starch granules are particles with a size range of 2–100 μm and are the form in which starch molecules – amylose and amylopectin – are organized within plants in a semi-crystalline fashion (Vandeputte and Delcour, 2004). When starch granules are heated in the presence of excess water, they swell and, eventually, gelatinize, with enough time and heat. Gelatinization is the irreversible process by which starch granules transform from their ordered semi-crystalline state to a disorganized amorphous state (Ai and Jane, 2015) and is characterised by loss of granule birefringence and increased suspension viscosity (Schirmer et al., 2015). Although gelatinization is typically done by heating starch granules, the same result can be achieved using high hydrostatic pressure (Schneider Teixeira et al., 2018) and can be affected by pH and osmolarity (Simonin et al., 2011). Gelatinization occurs gradually, both within each granule, and with all of the granules collectively in the sample. Gelatinization is an important process for improving the usability of starch and is used in various industries (Builders and Arhewoh, 2016; Ratnayake and Jackson, 2007). Although most aspects of the gelatinization process are well characterized and understood (Ai and Jane, 2015; Schirmer et al., 2015; Waigh et al., 2000), the changes to the internal macrostructure of starch through gelatinization have not been clearly elucidated.

It is well known that many types of starch have granules which can have an internal cavity or hole in their native state. These cavities have been reported in starch granules originating from rice (Baldwin et al., 1994; Sujka and Jamroz, 2013), wheat (Baldwin et al., 1994; Sujka and Jamroz, 2013), potato (Baldwin et al., 1994; Hall and Sayre, 1970; Sujka and Jamroz, 2013), sorghum (Huber and BeMiller, 2000), waxy corn (Chen et al, 2009, 2011), and normal corn (Chen et al, 2009, 2011; Huber and BeMiller, 2000; Sujka and Jamroz, 2013). Although it seems likely that these cavities observed in the native state are at least partly the result of drying (Baldwin et al., 1994), the exact origin remains a topic of discussion (Huber and BeMiller, 2000), and further work is needed. It is understood that the hilum region is an area of low organization (Błaszczak et al., 2005) and that gelatinization starts in the hilum region and proceeds radially to the periphery of the granule (Jane and Shen, 1993; Schirmer et al., 2013; Singh et al., 2003). It is likely that these two observations are related, and that gelatinization preferentially occurs in areas with less organized structure. As previously mentioned, the internal architecture changes that occur through the gelatinization process have

* Corresponding author.
E-mail address: maucoin@uwaterloo.ca (M.G. Aucoin).

https://doi.org/10.1016/j.heliyon.2020.e05294
Received 9 June 2020; Received in revised form 11 August 2020; Accepted 14 October 2020

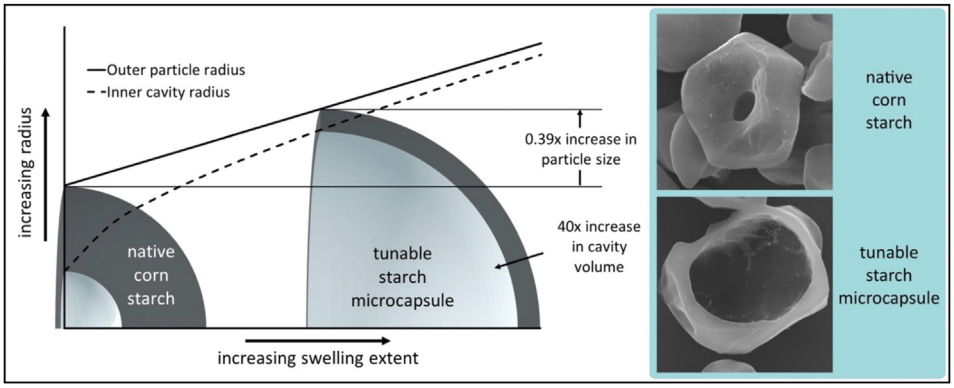

Figure 1. Graphical abstract.

been poorly characterized. Some research has observed an internal cavity in partially-gelatinized starch (Hall and Sayre, 1971; Schirmer et al., 2013), but no research has studied the progression of that internal cavity at different stages of gelatinization. Little is known about what is happening structurally inside a starch granule as it transitions from a highly organized semi-crystalline granule to a highly disorganized amorphous state through the gelatinization process. It is also worth noting that some research has characterized the remaining nonsoluble parts of fully-gelatinized starch granules, often referred to as "ghosts". These ghosts form when starch is gelatinized with little or no shear, producing structures which are hollow, highly swollen, fragile, and amylopectin-rich (Debet and Gidley, 2007; Gómez-Luría et al., 2017; Zhang et al., 2014).

In this paper, we have studied the swelling process as a result of partial gelatinization and the resulting structural changes that occur. We use the term "partial gelatinization" to refer to starch granules which have been swelled but would not be considered fully gelatinized, and we refer to these particles as starch microcapsules (SMCs). The swelling extent (i.e. how swelled the particles are) is characterized through measurement of the swelling power. The internal structure of the corn starch was observed at various stages of swelling through characterization with scanning electron microscopy, brightfield microscopy, polarizing light microscopy, and confocal laser scanning microscopy. In addition to achieving our objective of characterizing the swelling process, we also determined that the SMCs which we created can be modulated in terms of both the swelling extent and the internal cavity size through a simple heating process. Both the swelling process and how the internal cavity changes as a result of the swelling were also mathematically modeled and fit to our experimental data (see Figure 1).

2. Materials and methods

2.1. Materials

Normal corn (maize) starch was purchased from Sigma-Aldrich (S4126, Lot #: MKBT0621V) (Oakville, Canada). The apparent amylose content of the native starch was 27.8% as determined by the method of Williams et al. (1970). The moisture content was 14.2%, determined by the difference in weight as a fraction of the initial weight after drying for 16 h at 100 °C. FITC-dextran (MW 10,000) was purchased from Sigma-Aldrich.

2.2. Preparation of starch microcapsules (SMCs) through heating in water

The starch microcapsules (SMCs) were prepared through a simple heat-treatment process. Native corn starch (0.7 g, dry basis), as received from the supplier, was added with Milli-Q water (14 mL) in a centrifuge tube at a concentration of 5% w/w (native, dried starch basis). To swell the starch, the centrifuge tube was placed in a water bath at the required heating temperature (55–85 °C) for the required time (5–240 min) with stirring of the water bath with a magnetic stirrer. The height of the water in water bath was carefully controlled to also cause gentle agitation of the centrifuge tube. After the starch was swelled, the starch mixture was cooled immediately to 20 °C by placing the centrifuge tube in a cold-water bath. Unless the particles were to be sectioned, the particles remained in solution for further use.

2.3. Starch swelling power

To measure the swelling power, the centrifuge tube containing the mixture of starch (native granules or SMC particles) and water were centrifuged at 1000 g for 15 min based on the method reported by Kim and Huber (2013). The weight of the sediment after decanting the supernatant was then measured. The swelling power was calculated using Eq. (1):

$$\text{Swelling power} = \frac{\text{Weight of sediment (g)}}{\text{Dry basis weight of starch (g)}} \quad (1)$$

2.4. Soluble starch fraction

We calculated the fraction of soluble starch using the standard approach for starch solubility analysis (S. Wang and Copeland, 2012) with an alternate method of calculation as noted below. The decanted supernatant (from the swelling power measurement step) was added to a pre-weighed glass vial and placed in an air oven at 105 °C until at a constant weight (~24 h). The weight of the dried soluble starch was then measured, and the weight loss was used to calculate the amount of soluble starch in the supernatant. Since the volume of the supernatant is less than the volume of the water added initially – the result of interparticle and intraparticle water – the solubility was corrected by the ratio of these two volumes to account for this difference. This correction assumes that all water in the mixture has the same concentration of soluble starch, regardless of whether it is the supernatant or interparticle or intraparticle water. The solubility was calculated using Eq. (2):

$$\text{Soluble starch fraction} = \frac{\text{Weight of dried supernatent (g)} * \frac{\text{Initial water volume (mL)}}{\text{Supernatant volume (mL)}}}{\text{Dry basis weight of starch (g)}} \quad (2)$$

2.5. Starch granule size distribution

Starch particle sizes were measured using a laser particle sizer (Fritsch NanoTec Analysette 22, Fritsch GmbH, Idar-Oberstein, Germany) using static light scattering. The starch samples were suspended in water at a concentration of about 7% (w/w). The surface weighted mean diameter [D(3,2)] (i.e. Sauter diameter) was used as the representative

diameter. The surface weighted mean is the equivalent diameter of a sphere which has the same volume/surface area ratio.

2.6. Sectioning of starch for internal particle imaging with SEM

After the SMC preparation process, the sediment was frozen through immersion in liquid nitrogen. The sample was then mounted to a cold (-18 °C) metal disc using optimal cutting temperature (OCT) compound (VWR, Mississauga, Canada), which rapidly freezes to keep the sample in place. The sample was then sectioned, while still frozen, in 10 μm increments using a cryomicrotome (Shandon Cryomicrotome SME, Thermo, Mississauga, Canada) with a metal triple-facet cryomicrotome blade (VWR, Mississauga, Canada). The samples were then placed back in a -20 °C freezer until further use. The part of the pellet that was sectioned was not in contact with the OCT fluid.

2.7. Scanning electron microscopy (SEM) imaging of starch

The starch samples (native and SMC) were prepared through either a) acetone washing and vacuum drying or b) freeze drying to remove residual water. The dried starch samples were sprinkled onto double-sided carbon tape attached to the specimen stubs. Gold sputtering was performed for 120 s for an approximate coating thickness of 10 nm. The starch was then viewed using a scanning electron microscope (SEM, Quanta FEG 250, FEI, USA, 10–30 keV).

2.8. Optical imaging of starch

The starch samples (native and SMC) were placed on a glass slide, a small drop of water was added, and a coverslip was placed on top. The slide was then imaged using an optical microscope (Axioskop, Carl Zeiss, North York, Canada) at 50x magnification. Polarizing light images were taken using the same microscope with a set of cross polarizing light filters (Carl Zeiss, North York, Canada).

2.9. Fluorescent microscopy of starch

Starch samples (native and SMC) were added to a solution of fluorescein isothiocyanate conjugated with dextran (FITC-dextran) with a molecular weight of 10,000 g/mol at a concentration of 10 mg/mL and were left overnight at room temperature for loading of the particles. Right before imaging (~15–30 min before), each sample was placed on filter paper using a pipette to wick away excess liquid and then rinsed using a few drops of water. The starch was removed from the filter paper and placed on a microscope slide; a drop of water was added, and a coverslip was placed on top. Nail polish was used to seal between the edges of the coverslip and the slide to prevent evaporation and movement. Once the nail polish was dry (~5 min), the slide was placed on the microscope and images were taken using a confocal microscope (LSM 700, Carl Zeiss, North York, Canada) with illumination by the 488 nm laser using a 100x oil emersion objective.

2.10. Particle size and internal cavity analysis on SEM images

SEM images of sectioned particles were analyzed for particle dimensions in Photoshop (Adobe, San Jose, CA, USA) using the ruler tool. To calculate the particle diameter, the widest and narrowest diameters were measured and the two were averaged to calculate the average diameter for each particle. To calculate the internal cavity diameter, the shell thickness was first measured by averaging the thickest and the thinnest points of the particle shell and then calculated using Eq. (3):

$$\text{Internal cavity diameter} = \text{Particle diameter} - (2*\text{shell thickness}) \quad (3)$$

A total of eight particles for each particle type were analyzed. The theoretical equation for modeling the internal cavity size as a function of the particle size was fitted using the initial hole size (β_i).

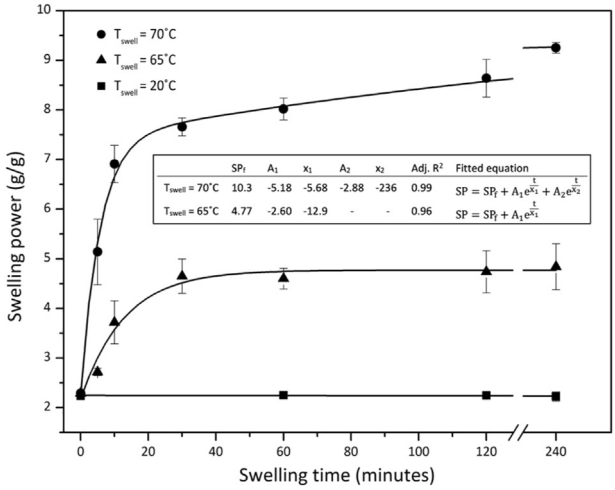

	SP_f	A_1	x_1	A_2	x_2	Adj. R^2	Fitted equation
T_{swell} = 70°C	10.3	-5.18	-5.68	-2.88	-236	0.99	$SP = SP_f + A_1 e^{\frac{t}{x_1}} + A_2 e^{\frac{t}{x_2}}$
T_{swell} = 65°C	4.77	-2.60	-12.9	-	-	0.96	$SP = SP_f + A_1 e^{\frac{t}{x_1}}$

Figure 2. The swelling power of corn starch at increasing swelling times with heating at 70 °C and 65 °C, and with a swelling control at 20 °C (n = 3, mean ± SD). Exponential functions were fitted to the data, with a two-phase function used for heating at 70 °C and a single-phase function used for heating at 65 °C. The fitted parameters (SP_f, final swelling power; A_1; x_1; A_2; and x_2) and equations are provided in the inset table.

2.11. Statistical analysis

Swelling power experiments were conducted in triplicate or quadruplicate, and values are reported as the mean ± SD. The data were fitted empirically to model the observed behaviour. Lines of best fit were created in Origin graphing and data analysis software (OriginLab, Northampton, MA, USA). For the exponential equation fits, the ExpGro2 and ExpGro1 functions were used, representing two-phase exponential growth and single-phase exponential growth, respectively. For the sigmoidal equation fit, the Hill1 function was used. For the linear equation fit, the Line function was used. For the second order polynomial equation fit, a polynomial function with an order of two was used. The equations and fitted parameters are given within each plot figure.

3. Results and discussion

3.1. Preparation of tunable starch microcapsules (SMCs)

3.1.1. Control of swelling power using swelling time

The tunability of the swelling extent was first studied through measuring the swelling power as a function of time (Figure 2). The swelling power was measured at various swelling times with heating at 65 °C and 70 °C and with no heating (at 20 °C) as a control. All subsequent preparations of SMCs were swelled for 30 min for two reasons: 1) 30 min allowed for the swelling processes to mostly plateau as seen in Figure 2, and 2) 30 min is also what other work has used to prepare swelled starch particles (Kumar et al., 2018; Ratnayake and Jackson, 2007; Shi et al., 2013; Wang et al., 2017). The swelling process can be modeled using a second order exponential curve as seen with the solid lines in Figure 2. A similar swelling profile was observed by Desam et al. with waxy maize starch (2018). Control of swelling time is one way to control the swelling extent of the SMCs.

3.1.2. Control of swelling power using swelling temperature

The effect of temperature on the swelling power was studied by creating SMCs through heating (for 30 min) at 55 °C (SMC55), 60 °C (SMC60), 65 °C (SMC65), 70 °C (SMC70), 75 °C (SMC75), 80 °C (SMC80), and 85 °C (SMC85) (Figure 3). As the heating temperature

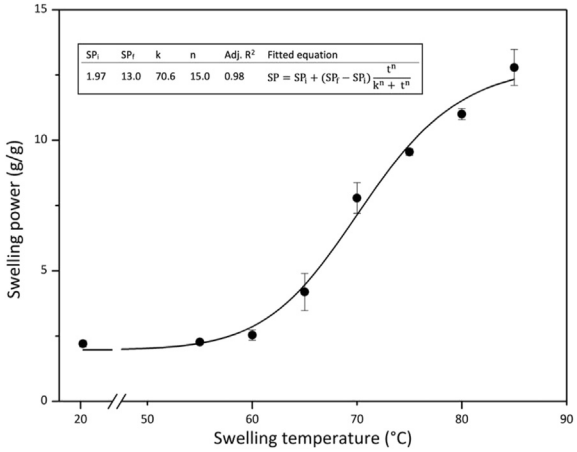

Figure 3. The swelling power (SP) of corn starch at increasing swelling temperatures (t) with heating for 30 min (n = 4, mean ± SD). A modified Hill equation was fitted to the data. The fitted parameters (SP_i, initial swelling power; SP_f, final swelling power; k; and n) and equation are provided in the inset table.

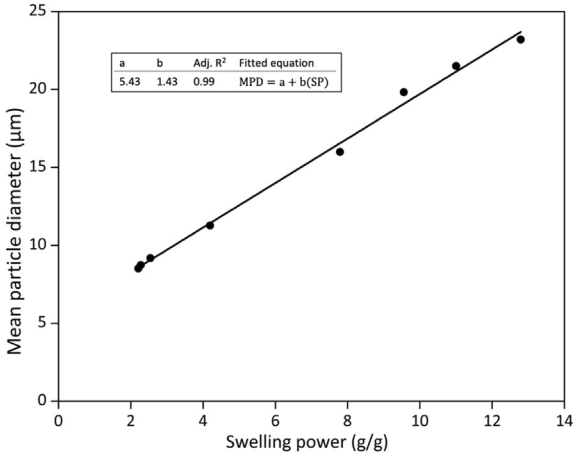

Figure 4. The effect of swelling power (SP) on the mean particle diameter (MPD). A linear equation was fitted to the data. The fitted parameters (a and b) and equation are provided in the inset table.

increases, the swelling power increases too. These results indicate that the most significant structural changes occur for the SMC65 and SMC70 samples because relative change from the native starch swelling power is the greatest for these two samples. The swelling process as a function of temperature can be modeled using a sigmoidal equation. It should be noted that the modified Hill equation as we have used it is only valid as a model up to 85 °C. A similar sigmoidal swelling profile was observed by Tester and Morrison when they measured swelling factor vs temperature for normal maize starch (Tester and Morrison, 1990). Control of swelling temperature is a second way to control the swelling extent of the SMCs.

3.1.3. Control of particle size using swelling power

As the swelling power increases, it is natural to conclude that the particle sizes must increase. Static light scattering (SLS) was used to determine particle diameters and to demonstrate the effect of swelling on the particle sizes (Figure 4). Increased swelling temperatures linearly correlates to increased particle sizes. Although laser light scattering data can be used to calculate various mean diameters, the mean Sauter diameter [D(3,2)] provided the best fit and thus was used. The Sauter diameter also showed the most similarity to diameters observed with

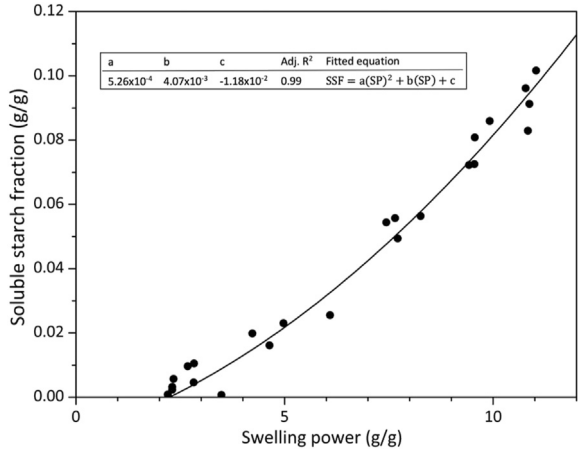

Figure 5. The effect of swelling power (SP) on soluble starch fraction (SSF). A second order polynomial function was fitted to the data. The fitted parameters (a, b, and c) and equation are provided in the inset table.

other microscopy methods. The correlation between the swelling power and diameter can be used to modulate the mean particle diameter. Native starch granules have a polydisperse particle size distribution, and so, as expected, the swelled SMCs likewise have a fairly polydisperse distribution (data not shown). It is worth noting that there are many active and passive methods for sorting microparticles while in solution (Sajeesh and Sen, 2014; Xi et al., 2017; Zhou et al., 2019), and it is expected that these SMCs would similarly be easily sortable based on their size to allow for a more monodisperse distribution if needed.

3.1.4. Control of soluble starch fraction using swelling power

As the particles swell and start to gelatinize, some of the polymer becomes solubilized. The soluble starch fraction (sometimes referred to by others as solubility or percent of leaching) can be plotted as a function of swelling power (Figure 5). This soluble starch is quite minimal at low swelling powers but does become increasingly significant as the swelling power increases. Our data can be fitted through a second order polynomial as indicated in Figure 5 by the solid line. The correlation between the swelling power and solubility can be used to control the extent of solubilization.

With normal corn starch, amylose preferentially leaches out (Doblado-Maldonado et al., 2017; Roger and Colonna, 1996). Further, the preferential leaching out of amylose in corn starch is more significant at lower heating temperatures: Doblado-Maldonado et al. (2017) observed leached material with 91.4% amylose content (determined through size exclusion chromatography) with heating at 90 °C, compared with 96.7% amylose content with heating at 70 °C (the native starch they used had an amylose content of 28.0%). It has also been suggested that that the leaching out of amylose is dependent on starch type (Vamadevan and Bertoft, 2020).

A single analysis of the amylose content on our results indicated that the soluble starch from preparing SMC70 had 68.6% amylose content, as determined through a colorimetric method (Williams et al., 1970), compared with 27.8% amylose content of the native corn starch, further supporting that amylose preferentially leeches out.

3.2. Characterization of starch microcapsules

3.2.1. Scanning electron microscopy

Scanning electron microscopy (SEM) provided clear images of the internal structure of the SMCs in a dry state. We observed that most native granules had an empty internal cavity (Figure 6a, d, and g). The internal cavities were primarily observed as being centred around the

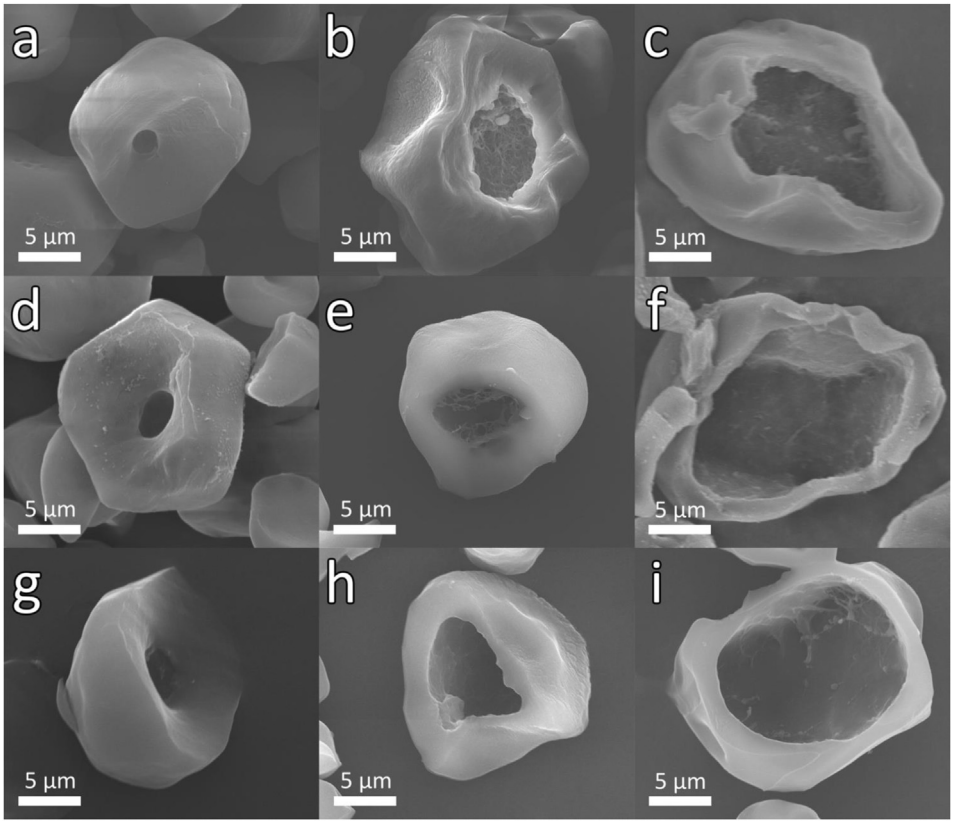

Figure 6. SEM images of sectioned native starch granules (a, d, and g), SMC65 particles (b, e, and h), and SMC70 particles (c, f, and i). Particles in images a, b, c, d, and f were acetone washed; e, g, h, and i were freeze dried. Scale bars indicate 5 µm.

hilum region. It has been reported that internal cavity formation is the result of drying (through creation of internal stresses) of the granules both in potato starch (Baldwin et al., 1994) and maize starch (Huber and BeMiller, 1997). The results in Figure 6a, d, and g also indicate that the internal cavity is empty, in agreement with work by Huber and BeMiller (2000). In contrast to our results, Gallant et al. suggested the space was filled with amorphous material (1997).

In the particles swelled at 65 °C (SMC65) (Figure 6b, e, and h), larger internal cavities were observed compared to the native corn starch granules. Particles showed some variation in the appearance of internal

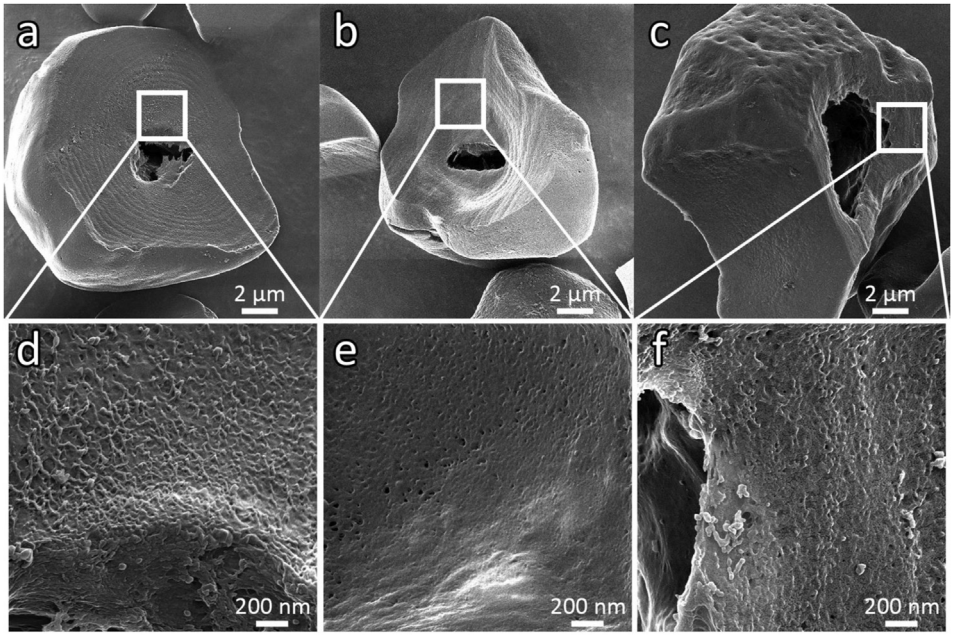

Figure 7. HIM images of sectioned native starch granules (a and d), SMC65 particles (b and e), and SMC70 particles (c and f). All particles were acetone washed. White boxes in the top images indicate the location of the zoomed-in bottom images. Images were taken using a Zeiss Orion Plus helium ion microscope. Scale bars indicate 2 µm (top row) and 200 nm (bottom row). Figure 7a and d are adapted and reproduced with permission from (Wulff et al., 2020).

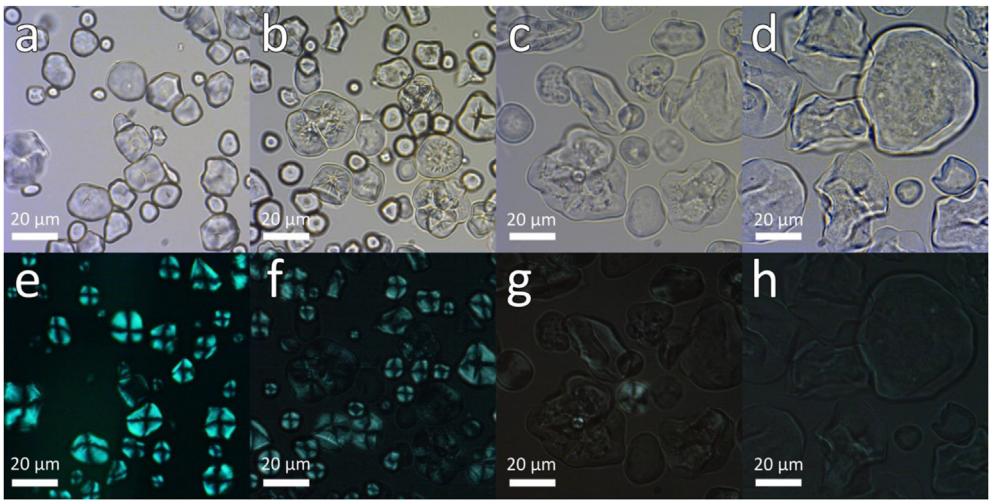

Figure 8. Microscopy images (brightfield, top; polarized light, bottom) of native corn starch granules (a and e), SMC60 particles (b and f), SMC65 particles (c and g), and SMC70 particles (d and h). For each sample type, the exact same particles were imaged for both brightfield and polarized images. Scale bars indicate 20 μm.

cavity surface roughness. Of particles which were sectioned and were oriented so that the interior could be seen, all showed an internal cavity. In the particles swelled at 70 °C (SMC70) (Figure 6c, f, and i), even larger internal cavities are seen compared with the SMC65 particles. With heating at 70 °C, the walls of the particles become quite thin as a result of particle expansion.

The primary mechanism for wall thinning and cavity growth is simply particle-swelling. With the assumption that the starch wall volume and density is conserved, the starch cavity volume can be modeled mathematically as the particle swells (see Section 3.3). As we have observed that solubilization also occurs with particle swelling, this solubilization must contribute either to wall thinning and cavity growth, to a decrease in density of the starch wall, or to both. However, if we assume that starch density is constant, when the effect of solubilization (using data and correlations in Figures 4 and 5) on internal cavity volume is calculated mathematically, it is seen that the effect is negligible (proof given in Figure 11).

Our results support the idea that the starch closest to hilum region consists of more loosely packed structure which is the most easily solubilized (Yang et al., 2016). Although there is still conflicting results regarding whether there is more amylose or amylopectin in the interior of starch granules (Bertoft, 2017), there is consensus that this interior region is more amorphous than the peripheral regions of the starch granule (Buléon et al., 1998; Vamadevan and Bertoft, 2015) and that this region gelatinizes most easily (Bogracheva et al., 1998).

3.2.2. Helium ion microscopy

Helium ion microscopy (HIM) is a relatively new characterization method which is capable of producing high-resolution images of starch, as we have previously reported (Wulff et al., 2020). The results in Figure 7 support what is seen in the SEM images (Figure 6). In native corn starch corn starch granules, growth rings (Figure 7a) and the surface morphology (Figure 7d) with a mesh-like structure are clearly seen. HIM images of SMC65 (Figure 7b and e) clearly show a distinct internal cavity similar what was seen with SEM. In addition, pore-like structures are seen in the wall of the particle. The images of SMC70 particles (Figure 7c and f) similarly supported what we saw observed with SEM. In Figure 7c, the wall of the SMC70 particle shows mesh-like features (as seen in Figure 7a) and pores (as seen in Figure 7b).

3.2.3. Optical microscopy

Brightfield images of the swelling process (Figure 8a – d) clearly show the increase in size as the particles are heated at higher temperatures and support the SEM and HIM results, but with particles which are fully wet and in solution. The particles also appear to become more translucent at they get larger. The SMC70 particles (Figure 8d) have a diameter which is about double compared to the native starch granules (Figure 8a), roughly in agreement with the quantitative results obtained using the laser particle sizer.

Polarizing light microscopy allows for insight into the crystallinity of the starch granules. These images show the transition from native corn (Figure 8e), which is birefringent (as indicated by the characteristic 'Maltese cross'), to nearly complete loss of birefringence when heated to 70 °C (Figure 8h). The 'Maltese cross' demonstrates radial organization within the starch granule and indicates a high degree of order inside the granules (Bertoft, 2017). Loss of birefringence is known to be associated with melting of crystallites (Li et al., 2013) and is one way to define gelatinization (Parker and Ring, 2001).

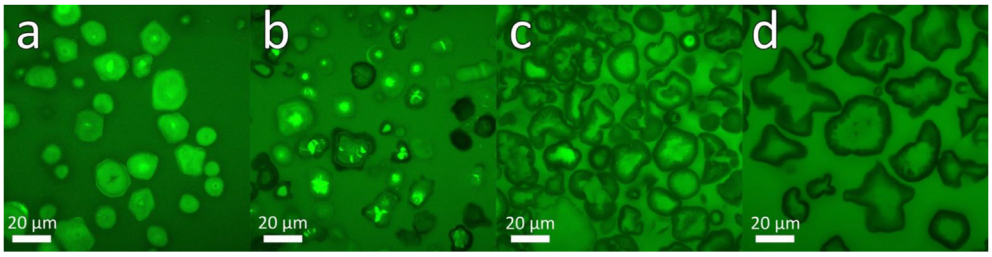

Figure 9. Confocal laser scanning microscopy images of native corn starch granules (a), SMC60 particles (b), SMC65 particles (c), and SMC70 particles (d). Scale bars indicate 20 μm.

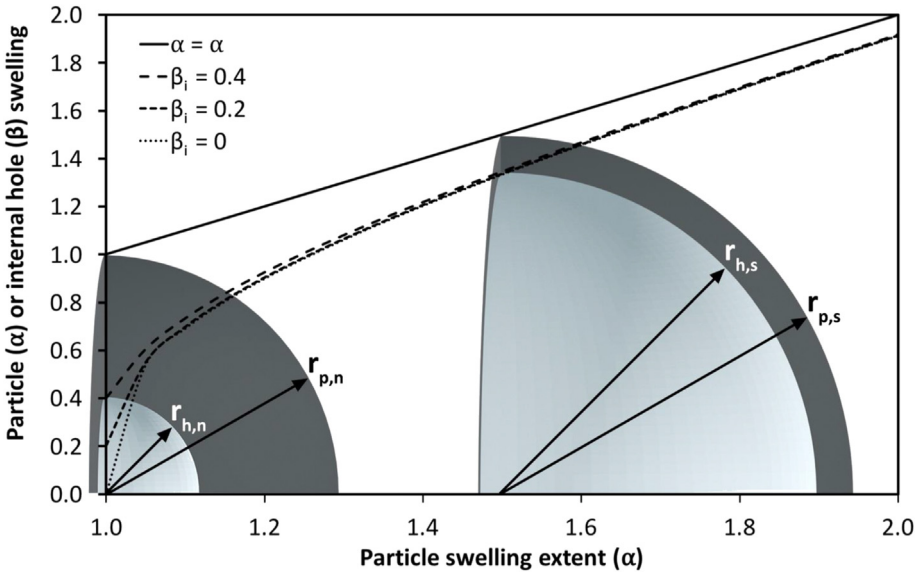

Figure 10. The effect of particle swelling on internal hole size can be seen by comparing the effect of increasing particle swelling extent (α) with various initial hole sizes (β_i) on swelled hole sizes (β). The superimposed particle section on the left indicates a native (n) starch granule demonstrating the radius of the hole (h) and of the outer particle surface (p), and the superimposed particle on the right indicates a swelled (s) starch microcapsule (SMC) demonstrating the same radii.

3.2.4. Confocal laser scanning microscopy

CLSM images (Figure 9) allowed for internal structures to be seen both in a wet state and without using a microtome to physically section the starch. FITC-dextran (MW 10,000) was chosen because it shows clear identification of features in starch granules and is not selective with respect to amylose or amylopectin. As noted by Schirmer et al., there is little information on the way in which various dyes interact with starch granules (2013). Based on our method of preparation, it was possible to qualitatively analyze the diffusion of the FITC-dextran after the particles had been washed with water.

Native corn starch (Figure 9a) showed some variation between particles with respect to dye localization. Some particles showed high fluorescence in the hilum region of the particles while others showed very low fluorescence there, in agreement with work by Dhital et al. (2013). This result seems to indicate that, of native granules that had an internal cavity in the hilum region, only some were permeable to the FITC-dextran, which could mean that only some granules have pores or channels which are large enough for FITC-dextran to diffuse all the way to the centre of the granule. A similar result was found by Achayuthakan et al. who observed higher permeation in rice starch with MW 4,000 FITC-dextran compared to MW 10,000 FITC-dextran (2012). In addition, of the particles which were fully permeable to FITC-dextran, the fluorescent intensity in the hilum region was very high. Based on the assumption that higher fluorescent intensity means higher concentration of FITC-dextran, this higher intensity indicated that the hilum region was empty which allowed for higher concentration of the dye. The reason for the lower fluorescence outside of the particles in Figure 9a – c was likely due to the water washing step which dilutes the FITC-dextran.

In the SMCs (Figure 9b – d), internal cavities and their expansion were clearly observed. Of particular interest is that the particles, particularly SMC60 and SMC65 particles, have varying internal fluorescence. When the particles were washed and placed on the microscope slide, the FITC-dextran likely started to diffuse out slowly. Presumably particles which displayed higher internal cavity fluorescence had a slower rate of diffusion out of the particles. Relative background fluorescence was brighter with the SMC images compared with the native granule image, likely as a result of the FITC-dextran which has diffused out of the particles. One final observation is the loss in circularity as the particles swell, which could be an indication of lower structural integrity of the wall.

3.3. Mathematical modeling of starch swelling

It is possible to mathematically relate swelled particles sizes to the size of the internal hole. Two assumptions must be made: 1) particles are spheres and 2) particle wall volume and density are conserved through the swelling process. The swelled microcapsule will have an internal hole radius ($r_{h,s}$) that is a function of the native granule outer particle radius ($r_{p,n}$), the native granule internal hole radius ($r_{h,n}$), and the swelled microcapsule outer particle radius ($r_{p,s}$); it can be calculated, through derivation from the equation relating the volume of a sphere to its radius using Eq. (4):

$$r_{h,s} = \sqrt[3]{(r_{p,s})^3 + (r_{h,n})^3 - (r_{p,n})^3} \tag{4}$$

Eq. (4) can also be written in an alternative dimensionless form which uses variables to describe the relative swelling extent (α) and the relative size of the internal cavity (β). α represents the ratio of swelled particle radius to native particle radius, and β represents the ratio of the swelled hole radius to the native particle radius (Figure 10). β_i represents the ratio of the initial (unswelled) hole radius to the native particle radius. These variables are calculated using Eqs. (5), (6), and (7):

$$\alpha = \frac{r_{p,s}}{r_{p,n}} \tag{5}$$

$$\beta = \frac{r_{h,s}}{r_{p,n}} \tag{6}$$

$$\beta_i = \frac{r_{h,n}}{r_{p,n}} \tag{7}$$

Thus, the dimensionless equation now takes the form in Eq. (8):

$$\beta = \sqrt[3]{\alpha^3 + \beta_i^{\,3} - 1} \tag{8}$$

When plotted (Figure 10), the relationship between α, β, and β_i can be clearly seen. The two superimposed model particles in Figure 8 demonstrate the swelling process for a granule with $\beta_i = 0.4$, with the left particle being a native granule and the right particle being a swelled microcapsule. A small change in the outer particle radius results in a large

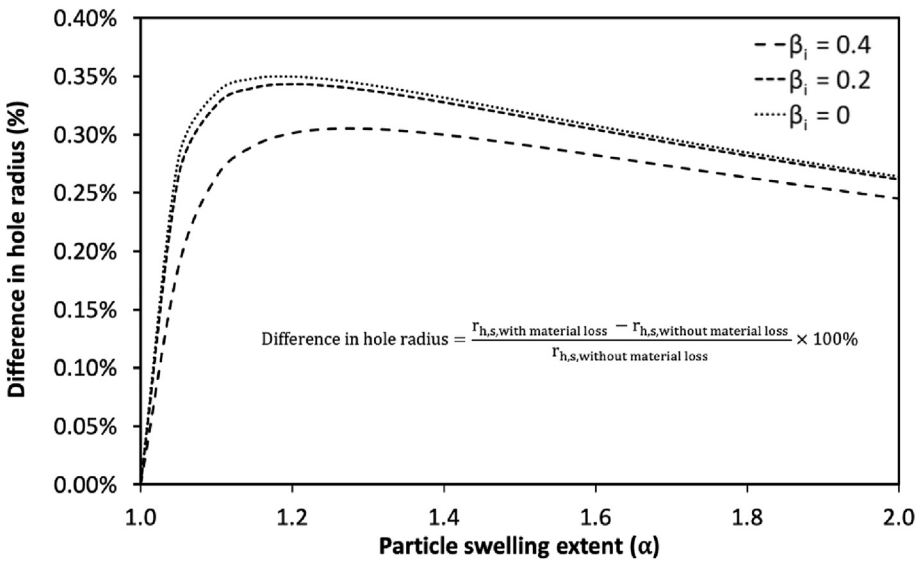

Figure 11. The effect of accounting for material loss when calculating the theoretical hole radius based on conservation of mass and density. The calculations are based on an initial particle radius of 4.25 μm, representative of native normal corn starch. The swelling power is calculated from the linear line of best fit (in Eq. (4)), and the fraction of soluble starch is calculated based on the second order polynomial line of best fit from the swelling power (in Eq. (5)). These calculations assume that a) both the solubilized and unsolubilized starch had the same density prior to any solubilization and b) the solubilized starch is only removed from the inner surface (i.e. the internal cavity side) of the particle.

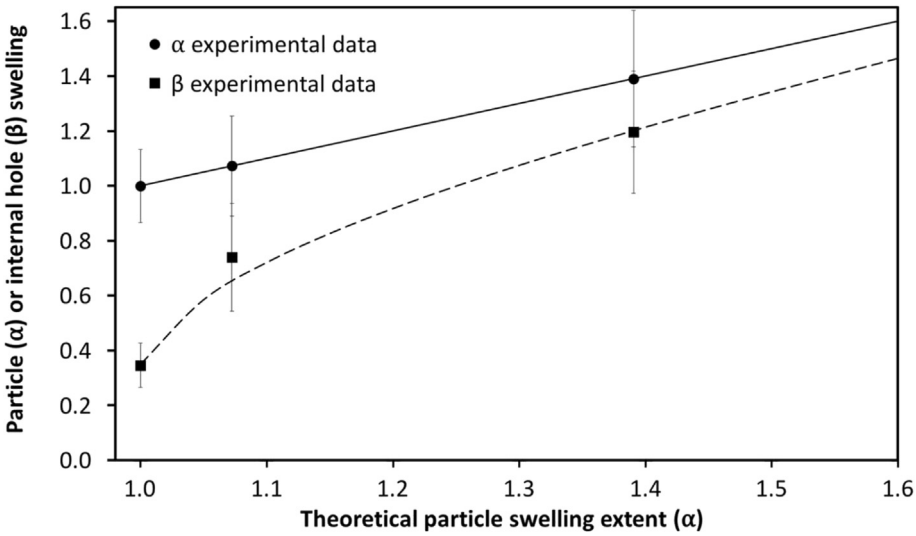

Figure 12. The experimental particle size and hole data fitted to the mathematical model. The fit for α represents the outer particle radius and the fit for β represents the internal hole radius (n = 8, mean ± SD).

change in the internal hole radius. It is also clear that the effect of the initial hole radius is negligible as the particle swells.

As indicated previously, the calculation of Eq. (8) the assumes conservation of particle wall (i.e. the shell) volume and density. However, even when the loss of soluble starch is accounted for by use of the correlations for swelling power and solubility in Figure 5, there is a less than 0.35% change in the hole radius at any given swelling power or initial hole size (Figure 11). As such, Eq. (8) provides a very close approximation without unnecessary complication.

3.4. Fitting of mathematical modeling with experimental data

The theoretical mathematical model in the previous section (Section 3.3) can be fit to particle size and hole size data based on SEM images of sectioned particles. Image analysis on native particles, SMC65 particles, and SMC70 particles yielded values for the relative swelling extent (α) and the relative internal hole size (β), which can be plotted and compared to the model equation. The measured β value for native particles gives $\beta_i = 0.35 \pm 0.08$; and this value is the only value needed to fit the model, as seen in Figure 12, which results in a close fit. The standard deviation is primarily a result of variation in particle and hole sizes and not measurement error.

Based on the experimental results, for SMC70 particles the average increase in particle radius is about 39% (i.e. $\alpha = 1.39 \pm 0.22$). Based on the fitted mathematical model, a 39% increase in the particle radius results in a relative internal hole size increase from 0.35 to 1.20, which means that internal cavity volume increases by a factor of 40x.

4. Conclusion

The starch granule swelling process in normal corn starch was studied through heating starch in an excess of water. Both the swelling temperature and the swelling time can be used to control the swelling extent of the particles, as measured by the swelling power. When the starch is swelled, there is a corresponding increase in the average particle diameter and in the amount of soluble starch, allowing for control of these properties too. The swelling process causes growth of the internal cavity, as clearly observed with SEM, HIM, and CLSM imaging. The growth of the internal cavity is primarily the result of particle expansion, and only a small increase in particle diameter corresponds to a large increase in the

internal cavity volume. The particle shell becomes thinner while the structural integrity of the particle appears to be largely maintained. The swelling process was modeled mathematically in close agreement with our experimental results.

Declarations

Author contribution statement

David Wulff: Conceived and designed the experiments; Performed the experiments; Analyzed and interpreted the data; Contributed reagents, materials, analysis tools or data; Wrote the paper.

Ariel Chan, Qiang Liu: Conceived and designed the experiments.

Frank X. Gu: Conceived and designed the experiments; Contributed reagents, materials, analysis tools or data.

Marc G. Aucoin: Conceived and designed the experiments; Contributed reagents, materials, analysis tools or data; Wrote the paper.

Funding statement

This work was supported by the Government of Canada through Agriculture and Agri-food Canada and also by the Natural Sciences and Engineering Research Council of Canada.

Competing interest statement

The authors declare no conflict of interest.

Additional information

No additional information is available for this paper.

Acknowledgements

The authors thank Elizabeth Donner for her technical support with analysis of amylose content and particles sizes and thank Lei Zhang for his assistance with creating the HIM images.

References

Achayuthakan, P., Suphantharika, M., Bemiller, J.N., 2012. Confocal laser scanning microscopy of dextran-rice starch mixtures. Carbohydr. Polym. 87 (1), 557–563.

Ai, Y., Jane, J.L., 2015. Gelatinization and rheological properties of starch. Starch - Stärke 67 (3–4), 213–224.

Baldwin, P.M., Adler, J., Davies, M.C., Melia, C.D., 1994. Holes in starch granules: confocal, SEM and light microscopy studies of starch granule structure. Starch - Stärke 46 (9), 341–346.

Bertoft, E., 2017. Understanding starch structure: recent progress. Agronomy 7 (3), 56.

Błaszczak, W., Fornal, J., Valverde, S., Garrido, L., 2005. Pressure-induced changes in the structure of corn starches with different amylose content. Carbohydr. Polym. 61 (2), 132–140.

Bogracheva, T.Y., Morris, V.J., Ring, S.G., Hedley, C.L., 1998. The granular structure of C-type pea starch and its role in gelatinization. Biopolymers 45 (4), 323–332.

Builders, P.F., Arhewoh, M.I., 2016. Pharmaceutical applications of native starch in conventional drug delivery. Starch Staerke 68.

Buléon, A., Colonna, P., Planchot, V., Ball, S., 1998. Starch granules: structure and biosynthesis. Int. J. Biol. Macromol. 23 (2), 85–112.

Chen, P., Yu, L., Simon, G.P., Liu, X., Dean, K., Chen, L., 2011. Internal structures and phase-transitions of starch granules during gelatinization. Carbohydr. Polym. 83 (4), 1975–1983.

Chen, P., Yu, L., Simon, G., Petinakis, E., Dean, K., Chen, L., 2009. Morphologies and microstructures of cornstarches with different amylose-amylopectin ratios studied by confocal laser scanning microscope. J. Cereal. Sci. 50 (2), 241–247.

Debet, M.R., Gidley, M.J., 2007. Why do gelatinized starch granules not dissolve completely? Roles for amylose, protein, and lipid in granule "ghost" integrity. J. Agric. Food Chem. 55 (12), 4752–4760.

Desam, G.P., Li, J., Chen, G., Campanella, O., Narsimhan, G., 2018. A mechanistic model for swelling kinetics of waxy maize starch suspension. J. Food Eng. 222, 237–249.

Dhital, S., Shelat, K.J., Shrestha, A.K., Gidley, M.J., 2013. Heterogeneity in maize starch granule internal architecture deduced from diffusion of fluorescent dextran probes. Carbohydr. Polym. 93 (2), 365–373.

Doblado-Maldonado, A.F., Janssen, F., Gomand, S.V., De Ketelaere, B., Goderis, B., Delcour, J.A., 2017. A response surface analysis of the aqueous leaching of amylose from maize starch. Food Hydrocolloids 63, 265–272.

Gallant, D.J., Bouchet, B., Baldwin, P.M., 1997. Microscopy of starch: evidence of a new level of granule organization. Carbohydr. Polym. 32, 177–191.

Gómez-Luría, D., Vernon-Carter, E.J., Alvarez-Ramirez, J., 2017. Films from corn, wheat, and rice starch ghost phase fractions display overall superior performance than whole starch films. Starch Staerke 69 (11–12), 1700059.

Hall, D.M., Sayre, J.G., 1970. Internal architecture of potato and canna starch - Part I: crushing studies. Textil. Res. J. 40 (3), 147–157.

Hall, D.M., Sayre, J.G., 1971. Internal architecture of potato and canna starch - Part II: swelling studies. Textil. Res. J. 41 (5), 404–414.

Huber, K.C., BeMiller, J.N., 2000. Channels of maize and sorghum starch granules. Carbohydr. Polym. 41 (3), 269–276.

Huber, Kerry C., BeMiller, J.N., 1997. Visualization of channels and cavities of corn and sorghum starch granules. Cereal Chem. J. 74 (5), 537–541.

Jane, J., Shen, J.J., 1993. Internal structure of the potato starch granule revealed by chemical gelatinization. Carbohydr. Res. 247, 279–290. Retrieved from: https://ac.els-cdn.com/000862159384260D/1-s2.0-000862159384260D-main.pdf?_tid=38bfd60d-1458-443a-a92b-d3f1c2eea86d&acdnat=1549479136_70f972bf9a44570993adb5ba65c6bcc3.

Kim, J.-Y., Huber, K.C., 2013. Corn starch granules with enhanced load-carrying capacity via citric acid treatment. Carbohydr. Polym. 91 (1), 39–47.

Kumar, L., Brennan, M., Zheng, H., Brennan, C., 2018. The effects of dairy ingredients on the pasting, textural, rheological, freeze-thaw properties and swelling behaviour of oat starch. Food Chem. 245, 518–524.

Li, Q., Xie, Q., Yu, S., Gao, Q., 2013. New approach to study starch gelatinization applying a combination of hot-stage light microscopy and differential scanning calorimetry. J. Agric. Food Chem. 61 (6), 1212–1218.

Liu, Q., 2005. Food carbohydrates: chemistry, physical properties, and applications. Food Carbohydr.

Parker, R., Ring, S.G., 2001. Aspects of the physical chemistry of starch. J. Cereal. Sci. 34, 1–17.

Ratnayake, W.S., Jackson, D.S., 2007. A new insight into the gelatinization process of native starches. Carbohydr. Polym. 67 (4), 511–529.

Roger, P., Colonna, P., 1996. Molecular weight distribution of amylose fractions obtained by aqueous leaching of corn starch. Int. J. Biol. Macromol. 19 (1), 51–61.

Sajeesh, P., Sen, A.K., 2014. Particle separation and sorting in microfluidic devices: a review. Microfluid. Nanofluidics 17 (1), 1–52.

Schirmer, M., Höchstötter, A., Jekle, M., Arendt, E., Becker, T., 2013. Physicochemical and morphological characterization of different starches with variable amylose/amylopectin ratio. Food Hydrocolloids 32 (1), 52–63.

Schirmer, Markus, Jekle, M., Becker, T., 2015, January. Starch gelatinization and its complexity for analysis. Starch Staerke 67 (1-2), 30–41.

Schneider Teixeira, A., Deladino, L., García, M.A., Zaritzky, N.E., Sanz, P.D., Molina-García, A.D., 2018. Microstructure analysis of high pressure induced gelatinization of maize starch in the presence of hydrocolloids. Food Bioprod. Process. 112, 119–130.

Shi, M., Gu, F., Wu, J., Yu, S., Gao, Q., 2013. Preparation, physicochemical properties, and in vitro digestibility of cross-linked resistant starch from pea starch. Starch Staerke 65 (11–12), 947–953.

Simonin, H., Guyon, C., Orlowska, M., de Lamballerie, M., Le-Bail, A., 2011. Gelatinization of waxy starches under high pressure as influenced by pH and osmolarity: gelatinization kinetics, final structure and pasting properties. LWT - Food Sci. Technol. (Lebensmittel-Wissenschaft -Technol.) 44 (3), 779–786.

Singh, N., Singh, J., Kaur, L., Sodhi, N.S., Gill, B.S., 2003. Morphological, thermal and rheological properties of starches from different botanical sources. Food Chem. 81 (2), 219–231.

Sujka, M., Jamroz, J., 2013. Ultrasound-treated starch: SEM and TEM imaging, and functional behaviour. Food Hydrocolloids 31 (2), 413–419.

Tester, R.F., Morrison, W.R., 1990. Swelling and gelatinization of cereal starches. I. Effects of amylopectin, amylose, and lipids. Cereal Chem. 67 (6), 551–557.

Vamadevan, V., Bertoft, E., 2015, January. Structure-function relationships of starch components. Starch Staerke 67 (1-2), 55–68.

Vamadevan, V., Bertoft, E., 2020. Observations on the impact of amylopectin and amylose structure on the swelling of starch granules. Food Hydrocolloids 103, 105663.

Vandeputte, G.E., Delcour, J.A., 2004. From sucrose to starch granule to starch physical behaviour: a focus on rice starch. Carbohydr. Polym. 58 (3), 245–266.

Waigh, T.A., Gidley, M.J., Komanshek, B.U., Donald, A.M., 2000. The phase transformations in starch during gelatinisation: a liquid crystalline approach. Carbohydr. Res. 328 (2), 165–176.

Wang, S., Copeland, L., 2012. New insights into loss of swelling power and pasting profiles of acid hydrolyzed starch granules. Starch Staerke 64 (7), 538–544.

Wang, W., Zhou, H., Yang, H., Zhao, S., Liu, Y., Liu, R., 2017. Effects of salts on the gelatinization and retrogradation properties of maize starch and waxy maize starch. Food Chem. 214, 319–327.

Williams, P.C., Kuzina, F.D., Hylnka, I., 1970. A rapid colorimetric procedure for estimating the amylose content of starches and flours. Cereal Chem.

Wulff, D., Aucoin, M.G., Gu, F., 2020. Helium ion microscopy of corn starch. Starch - Stärke 1900267.

Xi, H.D., Zheng, H., Guo, W., Gañán-Calvo, A.M., Ai, Y., Tsao, C.W., Tan, S.H., 2017. Active droplet sorting in microfluidics: a review. Lab Chip 17 (5), 751–771.

Yang, J., Xie, F., Wen, W., Chen, L., Shang, X., Liu, P., 2016. Understanding the structural features of high-amylose maize starch through hydrothermal treatment. Int. J. Biol. Macromol. 84, 268–274.

Zhang, B., Dhital, S., Flanagan, B.M., Gidley, M.J., 2014. Mechanism for starch granule ghost formation deduced from structural and enzyme digestion properties. J. Agric. Food Chem. 62 (3), 760–771.

Zhou, J., Mukherjee, P., Gao, H., Luan, Q., Papautsky, I., 2019. Label-free microfluidic sorting of microparticles. APL Bioeng. 3 (4), 041504.

Zhu, F., 2018. Relationships between amylopectin internal molecular structure and physicochemical properties of starch. Trends Food Sci. Technol.